Catalysis Today 423 (2023) 114293

Contents lists available at ScienceDirect

Catalysis Today

journal homepage: www.elsevier.com/locate/cattod

Electrocatalytic self-assembled multilayer structures based on thiolated Fc-DAB dendrimers: Determination of heavy metal ions by enzymatic inhibition

Evelyn Ospina [a], Beatriz Alonso [b,c], Carmen M. Casado [b,c], M. Pilar García Armada [a,*]

[a] Dpto. Ingeniería Química y Medio Ambiente, E.T.S.I.I., U.P.M., José Gutiérrez Abascal, 2, 28006 Madrid, Spain
[b] Dpto. de Química Inorgánica, Facultad de Ciencias, U.A.M., Cantoblanco, 28049 Madrid, Spain
[c] Institute for Advanced Research in Chemical Sciences (IAdChem), Universidad Autónoma de Madrid, Madrid 28049, Spain

ARTICLE INFO

Keywords:
Electrocatalysis
Biosensor
Self-assembled multilayer structure
Thiolated DAB dendrimers
Ferrocene
Enzymatic inhibition
Horseradish peroxidase
Heavy metals

ABSTRACT

The development of sensitive and rapid inhibition-based biosensors for monitoring trace levels of heavy metals such as lead and copper ions in environmental samples is of high interest. In this work, we describe the fabrication of HRP sensitive peroxide biosensors based on ferrocenyl thiolated DAB dendrimers as bonding-layer between electrodeposited and colloidal gold nanoparticles and compare their electrocatalytic properties with those of thiolated DAB homologues. The complete electrochemical, kinetic and analytical characterization of these new heavy metals' inhibition-biosensors are investigated.

1. Introduction

The industrialization and technological improvement activities can release considerable amounts of heavy metals to the environment, particularly to the aquatic ecosystem. The presence of heavy metals in the freshwater systems could be seriously hazardous to the biological systems due to their toxicity by the recalcitrance, biosorption and/or bioaccumulation, that can cause several life-threatening complications [1,2]. This work focuses on lead and copper ions because they may reach the environment due to conscious or unconscious human activities. Lead common sources are the PVC pipes in sanitation, agriculture, recycled PVC lead paints, jewellery, lunch boxes, etc. as well as the lead batteries. The common sources of copper are the fertilizers, tanning, and photovoltaic cells [3]. Both ions are related with adverse effects on the human metabolic process [4–6]. Lead binds to several enzymes causing their inhibition and is a risk factor for Alzheimer's disease, senile dementia, and is related with neuro-degenerative disease [3] because it penetrates through protective blood brain barrier. However, copper is an essential trace element in biological systems and living organisms because it is cofactor of at least 30 important enzymes. Copper is at the same time vital and toxic to biological systems, depending on their concentration. The deficiency of copper causes ischaemic heart disease, anaemia and bone disorders [7]. The copper excess causes DNA damage and interacts with lipid hydroxyperoxides to form malondialdehyde and 4-hydroxy-nonenal, which are considered to be carcinogens. Adreno-corticol hyperactivity, allergies, anaemia, arthritis, diabetes, kidney disorders and other diseases are related with the Cu^{2+} [3]. Therefore, the development of simple sensitive and rapid analytical methods for monitoring trace level of Pb^{2+} and Cu^{2+} in environmental samples is highly desirable. Several methods have been developed for the determination of these and others heavy metals, such as spectrophotometric [6,8,9], electrochemical [3,7,10–14], photo-electrochemical [15], atomic absorption spectrometric [4,16] and coupled plasma mass spectrometric [17] techniques.

In the last years, the enzyme inhibition caused by heavy metals has provided a new way to develop inhibition-based biosensors [18–20]. These devices are very attractive for environmental monitoring of heavy metals because of their advantages such as rapidity, effectiveness, simplicity, low detection limit, and selectivity. They offer the capability to detect single elements at low concentrations, enabling in situ analysis and low-cost screening procedures. Enzymes such as urease, [2], [4], horseradish peroxidase [5], [6], alcohol oxidase [7] and choline oxidase

* Corresponding author.
E-mail addresses: ej.ospina@alumnos.upm.es (E. Ospina), beatriz.alonso@uam.es (B. Alonso), carmenm.casado@uam.es (C.M. Casado), pilar.garcia.armada@upm.es (M.P.G. Armada).

https://doi.org/10.1016/j.cattod.2023.114293
Received 29 March 2023; Received in revised form 22 June 2023; Accepted 14 July 2023
Available online 17 July 2023

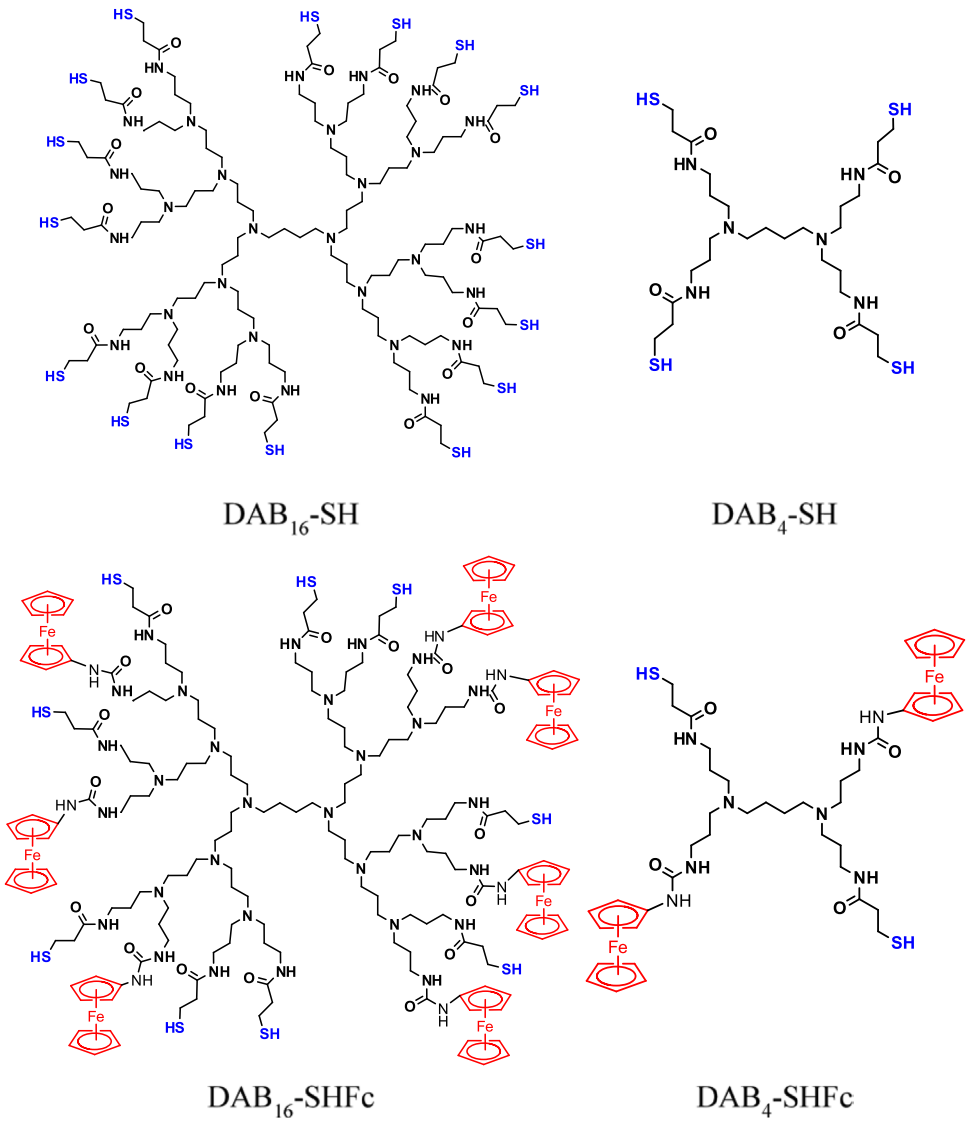

Fig. 1. Schematic representation of the dendrimer's structures.

[8], have been utilized, with mercury, copper, cadmium, and lead being the most frequently determined metals [5–7], [9], [10]. The development of sensitive and rapid inhibition-based biosensors for heavy metal detection promises to have a significant impact on environmental monitoring. However, several challenges remain in the detection of these heavy metals, requiring ongoing research and technological progress. Horseradish peroxidase (HRP) is one of more used enzymes due to their low cost, availability and easy immobilization. HRP has been widely used for the fabrication of hydrogen peroxide amperometric biosensors of second [21–24] and more recently, of third [25–27] generations due to the possibility of stablishing direct electrochemistry with the electrode material. Some heavy metal ions inhibit the ability of HRP to reduce H_2O_2 and therefore, an HRP peroxide sensor can be turned into an inhibition-based biosensor for the determination of these heavy metals. At present, several devices based on the HRP inhibition by heavy metal ions have been described [20,28–31].

Recently, we have reported a new HRP biosensor with a thiolated DiAminoButane based poly(propileneimine) dendrimer (DAB_{16}-SH) as bonding-layer between electrodeposited and colloidal gold nanoparticles (Au_c) of 16 nm, which form an electrocatalytic self-assembled layer (SAM) to the covalent immobilization and direct electrochemistry of HRP (HRP/Au_{c16}/-DAB_{16}-SH/AuNPs/GCE) [32]. This biosensor allows determining hydrogen peroxide at − 0.3 V vs. SCE with a fast response, in two linear ranges of 0–200 and 200–950 μM with sensitivities of 591.6 and 440.8 μA mM^{-1} cm^{-2} respectively, and detection limit of 0.11 μM.

On the other hand, it is known that ferrocene and its derivatives are excellent mediators and electrocatalysts in peroxidase-modified electrodes [33–35] and whose properties are enhanced for their synergy with AuNPs [27]. For this reason, we have considered interesting to study the effect of the substitution of some ferrocenyl groups for thiol ones on the improvement of the sensing properties of electrode surface. First generation of dendrimers with poly(propyleneimine) backbones and four peripheral ferrocenyl-urea [36] or thiol [37] units have been previously synthesized in our group.

In this work, we compare the catalytic properties of two generations of ferrocenyl thiolated DAB dendrimers with those of the thiolated DAB homologue, and demonstrate that these HRP sensitive peroxide biosensors can work as inhibition-based amperometric or impedimetric biosensors for Pb^{2+} and Cu^{2+}. The report includes the complete electrochemical, kinetic and analytical characterization of these new heavy metals' inhibition-biosensors.

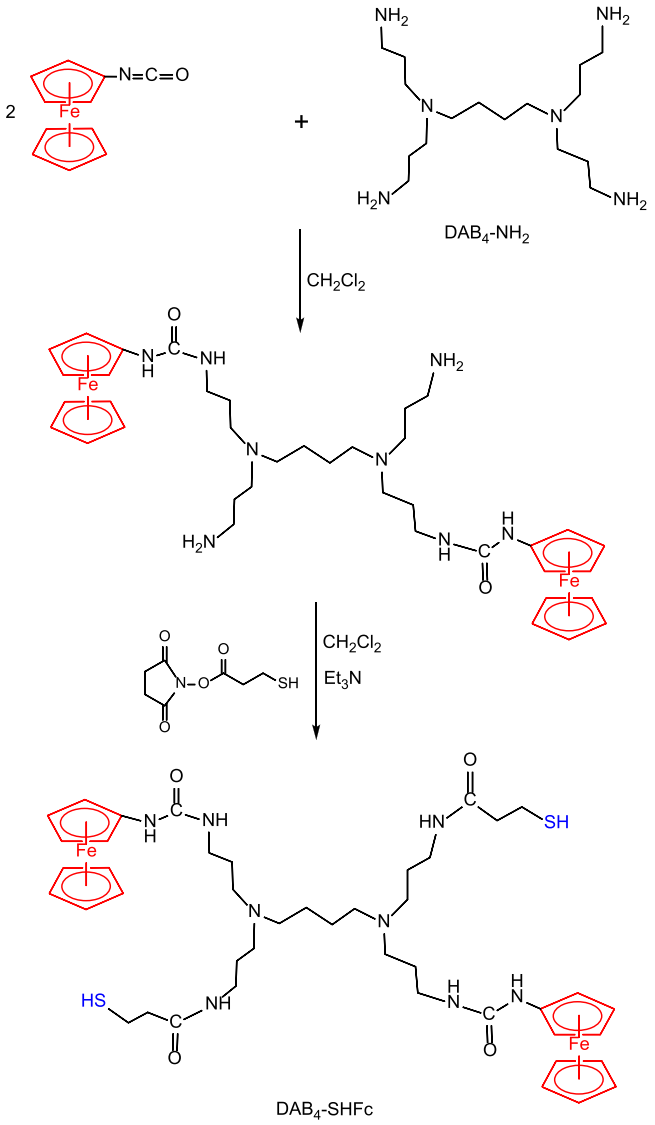

Scheme 1. Synthesis of DAB_4-SHFc.

2. Experimental section

2.1. Materials

In this work we have used the thiolated dendrimers of first and third generation with four (DAB_4-SH) and sixteen (DAB_{16}-SH) thiol terminal units respectively, synthesized as previously described [36,38], and ferrocenyl-thiolated dendrimers of first and third generation (Fig. 1) synthesized for the first time. All the synthesis reactions were performed under an inert atmosphere (N_2 or Ar) using standard Schlenk techniques. Solvents were dried by standard procedures over the appropriate drying agents and distilled immediately prior to use. The starting materials ferrocenyl isocyanate [39], and 3-mercaptopropanyl-N-hydroxysuccinimide ester [40], were prepared as previously described. The starting materials were used as received (Aldrich, Narchem) without any further purification. The dendritic polyamines DAB_4-NH_2 and DAB_{16}-NH_2 were purchased from Aldrich and were stripped three times with toluene in order to remove water prior to use. All the other chemicals were analytical grade and were used without further purification. Horseradish peroxidase (HRP, 222 units mg^{-1}), $HAuCl_4.3\,H_2O$, colloidal gold nanoparticles (5 nm), $Pb(NO_3)_2$ and $Cu(NO_3)_2$ were purchased from Sigma-Aldrich. The hydrogen peroxide solutions were previously normalized by the permanganate titration method. Ultrapure water was used for preparation of the buffers and standards, and for electrochemistry.

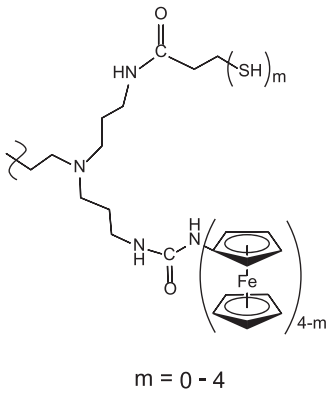

Fig. 2. Mixture of dendritic molecules, DAB_4-SHFc.

2.2. Instruments

All electrochemical measurements were carried out using an Eco-chemie BV Autolab PGSTAT 12. The experiments were performed in a conventional three-electrode cell at 20–21 °C with a GC disk of 3 mm diameter as working electrode, a Pt wire as auxiliary electrode and a saturated Calomel (SCE) as reference electrode. In the steady-state measurements, an Autolab rotating-disc electrode was used. The amperometric measurements were performed in 0.1 M $NaClO_4$/0.01 M phosphate buffer pH 7.0 (PBS) as supporting electrolyte. All solutions were deoxygenated by bubbling high-purity nitrogen for at least 15 min. The electrochemical impedance spectroscopy (EIS) studies were carried out on at 0.2 V vs. Ag/AgCl electrode, into the frequency range of 0.1–10,000 Hz, with 10 mV AC perturbation, in a 0.1 M KCl solution containing 10 mM of $K_3Fe(CN)_6/K_4Fe(CN)_6$ (1:1). The NMR spectra were recorded on a Bruker AMx-300 spectrometer. Chemical shifts are reported in parts per million (δ) with reference to residual solvent resonances. The MALDI-TOF mass spectrum were obtained using a Reflex III (Bruker) mass spectrometer equipped with a nitrogen laser emitting at 337 nm. The matrix was ditranol. The scanning electron microscopy (SEM) images were obtained with a JEOL JSM 6400.

2.3. Synthesis and characterization of ferrocenyl dendrimers

Ferrocenyl thiolated dendrimers have been prepared by following the same procedure. The synthesis of DAB_4-SHFc is shown in Scheme 1 as a representative example.

A highly diluted dichloromethane solution of ferrocenyl isocyanate was added dropwise to a vigorously stirred solution of 2 equiv. of DAB-NH_2 dendrimer in a large volume of dichloromethane and stirred for 20 h. Then, triethylamine was added, followed by a solution containing N-hidroxysuccinimide-3-mercaptopropanyl in dichloromethane. The mixture was stirred for three days (DAB_4-SHFc) or six days (DAB_{16}-SHFc) at room temperature. After removal of the solvent under reduced pressure and the appropriate workup (the resulting brawn residue was washed several times with hexane, then dissolved in dichloromethane and precipitated in hexane), the final products, were isolated as orange solids. The ^1H NMR spectra (300 MHz, DMSO-d_6) show the pattern of resonances in the range 4.5–3.8 ppm characteristic of the unsubstituted and substituted cyclopentadienyl ligands in the ferrocenyl moieties. The protons of the amide and urea groups appear at 8.0, 7.7 and 6.1 ppm respectively, and the resonance of the thiol group is observed at 1.2 ppm. As expected, the isolated metallodendritic species consist of mixtures of dendrimers with different ratios of the organometallic/thiol end groups on the surface (Fig. 2), which was corroborated by mass spectrometry.

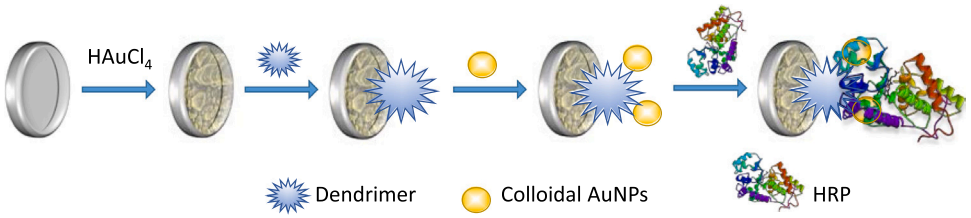

Scheme 2. Sensor fabrication steps: electrodeposition of AuNPs on the GCE surface, covalent anchorage of dendrimer, modification by colloidal AuNPs and covalent bonding of HRP.

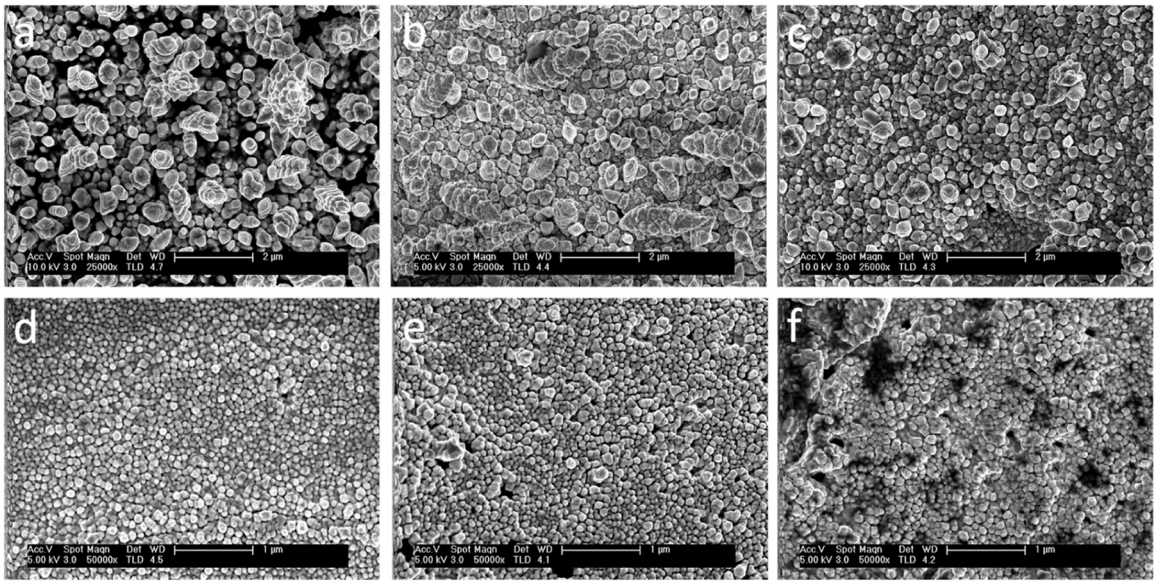

Fig. 3. SEM micrographs of a Pt wire covered with (a) electrodeposited AuNPs (9 cycles), (b) DAB_{16}-SH and (c) DAB_4-SH anchored to AuNPs (9 cycles). (d) Idem of electrodeposited AuNPs (3 cycles), (e) DAB_{16}-SHFc and (f) DAB_4-SHFc anchored to AuNPs (3 cycles) layer.

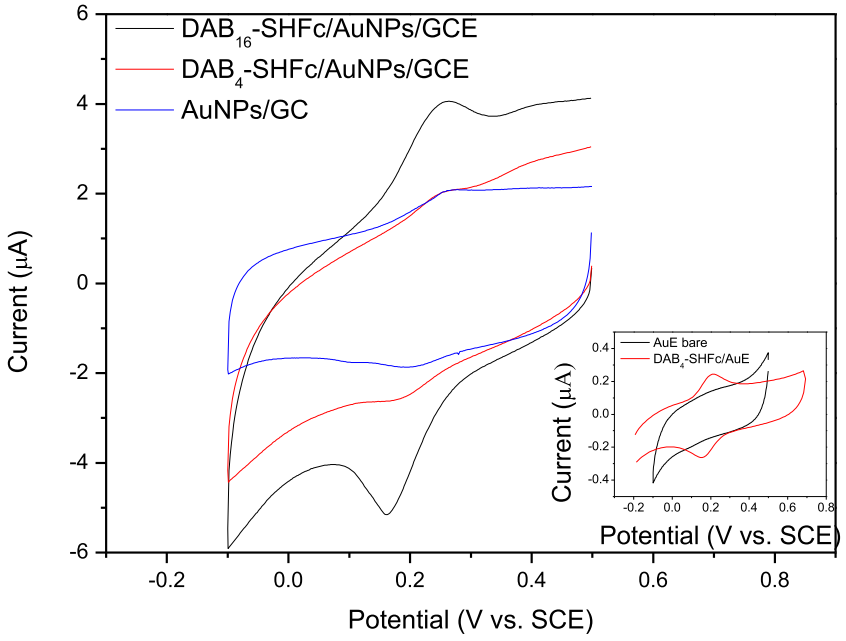

Fig. 4. Cyclic voltammograms of GCE modified in the two first steps of the SAMs preparation: AuNPs/GCE (blue line), DAB_4-SHFc/AuNPs/GCE (red line) and DAB_{16}-SHFc/AuNPs/GCE (black line). Inset: Bare gold disk electrode and the same modified with DAB_4-SHFc (black and red lines, respectively). All measured in PBS at scan rate 50 mV s^{-1}.

2.4. Preparation of modified electrodes

The GC disk electrodes were previously polished using 0.1 μm of alumina powder and rinsed in ultrapure water in an ultrasonic bath. The DAB-SH modified electrodes were prepared in the same way as previously described [32]. Briefly, the first layer was formed by electrodeposited AuNPs (nine cycles of potential between 0.2 and −0.4 V vs SCE in a 10 mM $HAuCl_4$ deaerated solution at 20 mV s^{-1} scan rate). Next, DAB-SH dendrimers were linked to the first layer maintaining 0.8 μL of a dendrimer aqueous solution (10^{-4} mM approx.) onto the AuNPs-electrode surfaces during 3 h at room temperature. As these dendrimers are not soluble in water, to prepare the DAB-SHFc modified electrodes the AuNPs-electrode was dipped in a DAB-SHFc 10^{-4} mM dichloromethane solution for 48 h to form the Au-S covalent bonds. In relation with the AuNPs coverage, in this case, the best results were obtained with a thinner coverage of AuNPs of three potential cycles measured in the same conditions of potential and scan rate than those used by the DAB-SH electrodes. Finally, all the modified electrodes thus prepared were dipped in the corresponding colloidal gold NPs, Au_c, suspension for 15 h. The Au_{c16} (16 nm) and Au_{c41} (41 nm) were synthesized according to the Turkevich method [41–43], with citrate as reductor. For the enzyme immobilization, the modified electrodes, washed with deionized water, were dipped in a phosphate buffer pH 7.0 solution containing 1.0 mg mL^{-1} of HRP at room temperature for 4 h. After this period, the biosensors were rinsed with the phosphate buffer and stored in the buffer solution at 4 °C when not in use. The preparation procedure is described in Scheme 2.

3. Results and discussion

3.1. Morphological, electrochemical and kinetic characterization of electrodes

Fig. 3 shows the SEM micrographs of the surfaces obtained throughout the two first preparation steps where the uniform coatings on the gold deposits are appreciable in b, c, d and e micrographs. Unfortunately, it has not been possible to achieve clear and sharp images of the colloidal nanoparticles incorporation due to the poor stability of the dendrimers under the SEM measurement conditions (Fig. 3f). However, we have included two micrographs of this stage in the supplementary material, in which some 16 nm AuNPs can be observed on the DAB_{16}-SH dendrimer (Fig. S1a) and those of 5 nm on the DAB_4-SHFc dendrimer (Fig S1b) could be intuited but are not evident.

The electrochemical characterization of DAB-SH modified electrodes was carried out in a previous work [32]. As expected, the voltammetric profile of the electrodeposited AuNPs (3-cycles) is similar to the 9-cycles coverage, but shows some differences due to the less amount of gold deposited. Fig. S2 shows an anodic broad wave at 0.880 V, corresponding to overlap of the peaks at 0.829 V and 0.986 V, and a cathodic peak at 0.450 V corresponding to the formation and reduction of the gold oxides at pH 7.0 [44,45]. With this coverage, the characteristic system of AuNPs is also visible at around 0.20 V [46–48]. The obtained average AuNPs surface, estimated from the coulombic integration of the cathodic waves of gold oxide and the widely accepted conversion factor of 390 μC/cm^2 [2,49,50] was 0.211 cm^2.

Fig. 4 shows the CVs of a GCE modified with AuNPs and DAB_4-SHFc and DAB_{16}-SHFc, compared with a gold electrode bare and modified with DAB_4-SHFc. As it can be seen, the AuNPs coverage shows the typical quasi-reversible system attributed to the oxide formation and reduction on the gold surface, with $E_a = 0.253$ V and $E_c = 0.198$ V. The presence of ferrocene could change the chemical and electrochemical properties in comparison with those of the DAB-SH dendrimers and their incorporation to the SAMs must show the ferrocene electrochemical system. Indeed, the Fc system is visible on the Fc-modified gold disk electrode but remains coupled with the AuNPs system at the same potential, showing a catalytic reduction wave, at least for the DAB_4-SHFc dendrimer. DAB_{16}-SHFc contains many more ferrocenyl units and not all of them are in contact with the AuNPs, so it also shows an oxidation peak, probably because the coupled reduction does not reach all the ferrocenyl units, and some electron transfers occur through the dendrimers to the electrode. In fact, the anodic peak area is 25% lower than the cathodic one, indicating that the coupled oxidation reaction partially occurs Table 1.

Table 1
Electrochemical and kinetic results.

Electrode	E^0 (V)	n	α	k_s (s^{-1})
DAB_4-SHFc/AuNPs/GCE	0.206	1.10	0.451	688
Au_{c5}/DAB_4-SHFc/AuNPs/GCE	0.198	1.03	0.489	1709
Au_{c16}/DAB_4-SHFc/AuNPs/GCE	0.184	1.00	0.489	1374
Au_{c41}/DAB_4-SHFc/AuNPs/GCE	0.182	0.96	0.505	1062
DAB_{16}-SHFc/AuNPs/GCE	0.207	1.03	0.494	735
Au_{c5}/DAB_{16}-SHFc/AuNPs/GCE	0.188	1.07	0.491	1359
Au_{c16}/DAB_{16}-SHFc/AuNPs/GCE	0.200	0.99	0.526	1299
Au_{c41}/DAB_{16}-SHFc/AuNPs/GCE	0.183	1.00	0.490	1229

The α and n values were estimated from $W_{1/2}$ measured at 700 mVs^{-1}
The results are the mean of 5 electrodes

Next, in order to determine the effect of the colloidal AuNPs on the electrode surface, we studied the dependence of peak potential and current on the scan rate. Fig. 5 shows the cyclic voltammograms of all types of modified electrodes, with and without colloidal gold nanoparticles of different sizes at several scan rates (v). All the modified electrodes present cathodic and anodic shifts as the scan rate increases, following the Laviron's model [51]. According to this model, when the scan rate tends to infinity, the peaks tend to irreversibility and the cathodic width at mid-height, $W_{1/2}$ becomes equal to $62.5/\alpha n$ mV, while the anodic one is $62.5/(1-\alpha)n$ mV, being α the electron-transfer coefficient and n the number of electrons exchanged. This relation allows us to estimate α and n. The Laviron's model also allows estimating the apparent homogeneous rate constant, k_s. In our case, all the modified electrodes showed a difference between the anodic and cathodic peak potentials, ΔE_p, less than $200/n$ mV. In these cases, the model let to calculate k_s from the supplied data for $\alpha = 0.5$ (with a relative error at the most of about 6% when $0.3 < \alpha < 0.7$), which polynomial fit ($R^2 = 0.9992$) is:

$$Fnv/RT\ k_s = 0{\cdot}0003\Delta Ep^2 + 0{\cdot}0047\Delta Ep + 0{\cdot}491$$

Where F is the Faraday constant, n is the number of electrons involved, T is the absolute temperature, and R is the gas constant. Table I shows the electrochemical and kinetic parameters obtained for the DAB-SHFc modified electrodes.

As can be seen, the obtained values for n and α are close to 1 and 0.5 respectively for all the prepared electrodes and the k_s values have experimented a very considerable increase compared to dendrimers without ferrocene [32]. This fact confirms the synergy that occurs between ferrocenyl groups and AuNPs. Likewise, we can affirm that the best composition is Au_{c5}/DAB_4-SHFc/AuNPs/GCE, with higher k_s, indicating that this electrode provides the faster electron transfer. The small differences in E^0 can be attributed to the inhomogeneity of the electrode surfaces due to differences in the Au_c orientation in the different configurations. The linear relationship of the anodic and cathodic peak currents with the scan rate is typical for surface-immobilized couples (insets in Fig. 5).

Electrochemical impedance spectroscopy (EIS) closes the electrochemical analysis, allowing us to study the interface electrode-electrolyte properties. An equivalent circuit models the electrode-electrolyte interfaces. The equivalent circuit consists of at least the elements: the charge-transfer resistance, R_{CT}, the double layer capacitance, C_{dl}, the Warburg impedance, Z_W, resulting from the ion diffusion from the bulk electrolyte to the electrode interface and the resistance of the electrolyte R_s [52]. In the case of rough electrode surfaces, the system turns away from the ideal capacitive behaviour and C_{dl} does not

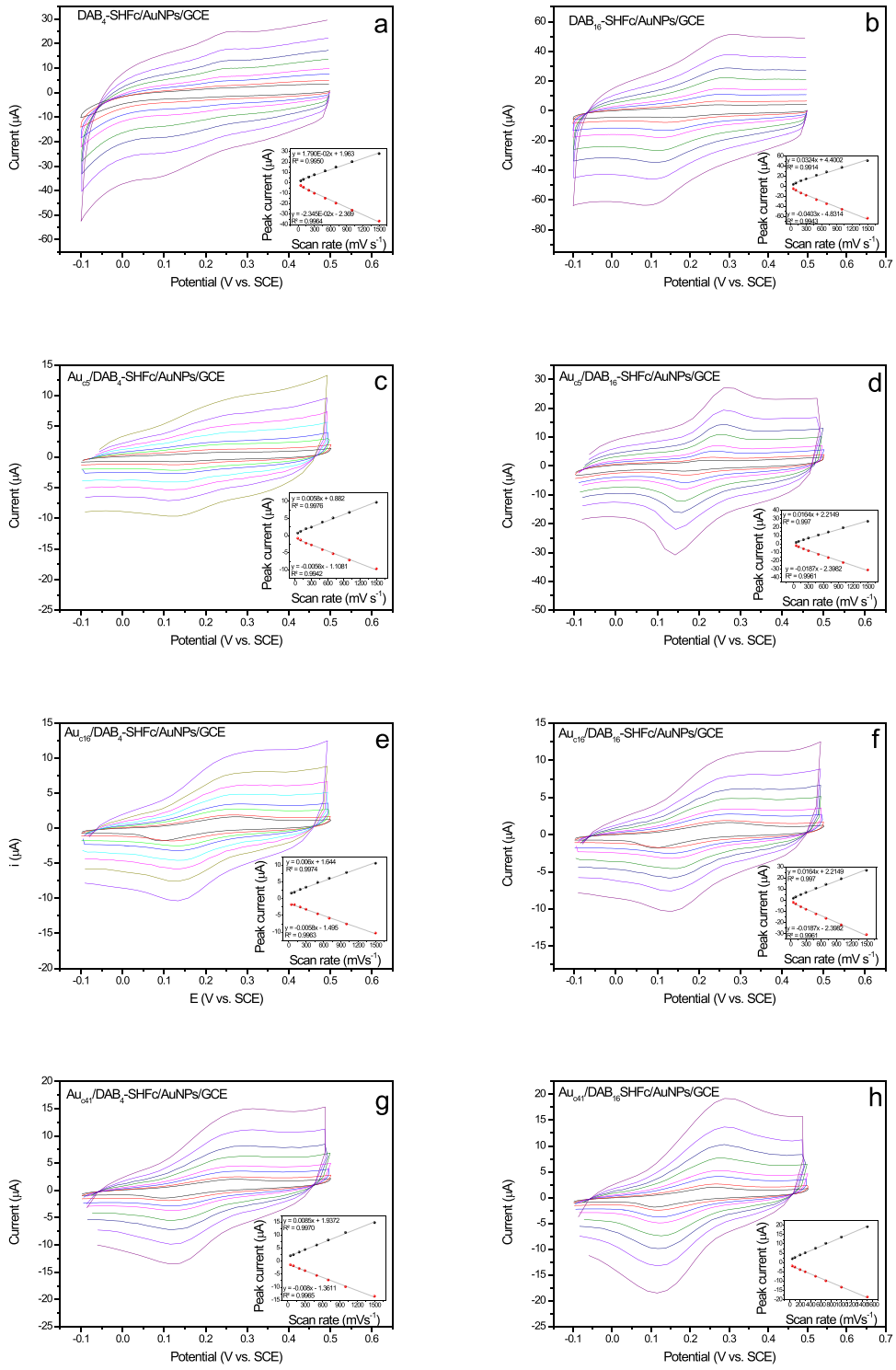

Fig. 5. Dependence of the peak current on the scan rate (50, 100, 200, 300, 500, 700, 1000 and 1500 mV s^{-1}) for all the modified electrodes in PBS. Insets: corresponding dependence of *ip* on *v* in the same conditions.

correctly describe the electronic properties of the interface. In these cases, a constant phase element, C_{PE}, is more adequate because reflects the electrode inhomogeneity. The element C_{PE} is defined as $C_{PE} = A^{-1}(jw)^{-N}$, where N indicates the deviation from the Randles model and takes values between 0.5 and 1. If N tends to 1, the coefficient A tends to C_{dl}.

In order to calculate R_{CT} and C_{dl}, the impedance imaginary part vs. the impedance real part plot (Nyquist plot) is widely used. This plot consists of a semi-circular part at high frequencies, whose diameter represents R_{CT}, and a linear part at low frequencies characteristic of systems with diffusion-controlled current. Fig. 6 displays the Nyquist plots obtained for the three main stages of preparation of the best electrodes of each type. Table 2 collects the results from the fit and simulation by the corresponding equivalent circuits (The whole results are showed in Figs. S3 and S4) for the DAB-SHFc electrodes. These data can be compared with the previously published corresponding to the DAB-SH electrodes [32].

The results indicate, firstly, that the conductivity is high in all the

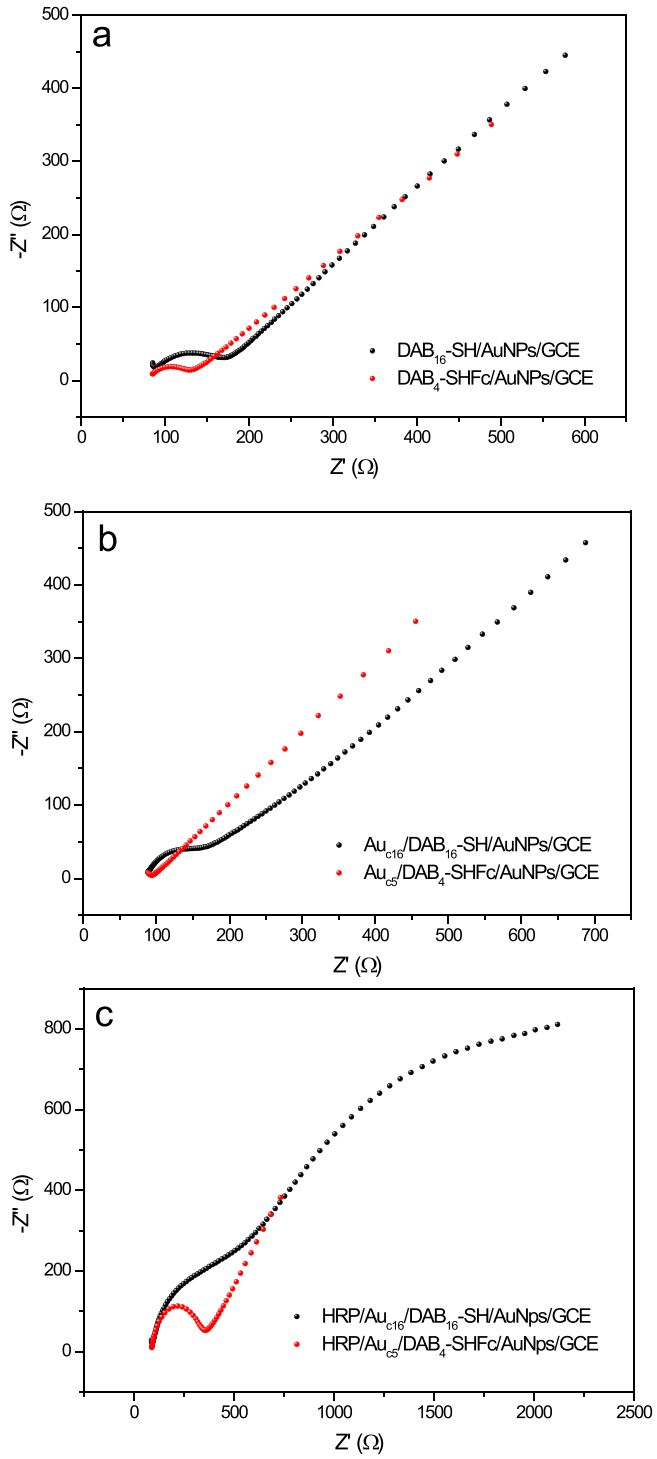

Fig. 6. Nyquist plots of (a) the DAB_{16}-SH/AuNPs/GCE and DAB_4-SHFc/AuNPs/GCE electrodes, (b) Au_{c16}/DAB_{16}-SH/AuNPs/GCE and Au_{c5}/DAB_4-SHFc/AuNPs/GCE electrodes, and (c) HRP/Au_{c16}/DAB_{16}-SH/AuNPs/GCE and HRP/Au_{c5}/DAB_4-SHFc/AuNPs/GCE, all of them obtained in $K_4[Fe(CN)_6]/K_3[Fe(CN)_6]$ 10 mM solution.

layers of the biosensors. However, they allow us to ensure that the conductivity improves when the ferrocenyl dendrimer is used, as expected, due to the lower conductivity of the thiolated-dendrimer layer in comparison with the ferrocenyl dendrimer. The low conductivity of the HRP [53,54] is responsible for the decrease in the biosensor conductivity, which indicates that the enzyme has been successfully assembled as last layer. The appearance of a second semi-circle at low frequencies

Table 2
Electrochemical impedance spectrometry results.

Electrode	R_{CT} (Ω)	*CPE* (μF)	*N*	k^0 (cm s^{-1})
DAB_4-SHFc/AuNPs/GCE	51	16.71	0.751	7.46×10^{-3}
Au_{c5}/DAB_4-SHFc/AuNPs/GCE	49	110.71	0.341	7.80×10^{-3}
HRP/Au_{c5}/ DAB_4-SHFc/AuNPs/GCE	253	5.11	0.893	1.50×10^{-3}

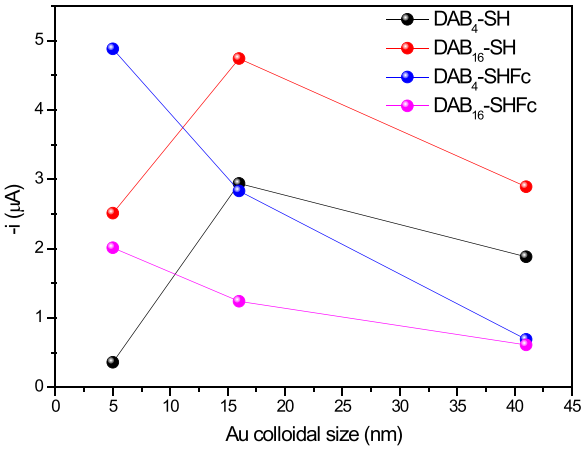

Fig. 7. Cathodic current obtained with the four types of biosensors as a function of the Au colloidal nanoparticles size in presence of hydrogen peroxide 100 μM in deaerated PBS at applied potential of − 0.3 V vs. SCE.

for the DAB-SH biosensor indicates that the electrochemical reaction occurs under the HRP layer and therefore, the electroactive material must reach the surface through different ways. This effect does not occur at the DAB-SHFc biosensor, indicating that the biosensor surface is more permeable. On the other hand, we can obtain the electron transfer constant k^0 from the equations: $R_{CT} = RT/nFi_0$, and $i_0 = nFAk^0C$ [55], where A is the electrode area (the area of 0.07 cm^2 has been used as reference for all the electrodes) and C is the bulk concentration of the redox probe in mol cm^{-3}. The electron transfer constants k^0 (Table 2) obtained for the DAB-SHFc electrodes are higher than those of DAB-SH devices, demonstrating the improvement of the charge transfer process of the probe redox system.

3.2. Hydrogen peroxide biosensors

The behaviour of DAB-SH electrodes as peroxide biosensors was previously studied in detail [32], obtaining the best results with HRP/Au_{c16}/DAB_{16}-SH/AuNPs/GCE (DAB-SH biosensor), showing a sensitivity of 590.0 μA mM^{-1} cm^{-2}, into a dynamic range of 0.4 – 200 μM at − 0.3 V working potential, and with limit of determination (LOD) of 20 nM. However, to corroborate the results of the kinetic and electrochemical studies, in Fig. 7 we show the results of current intensity obtained with the four types of modified electrodes, each with the three different sizes of colloidal gold nanoparticles. As it can be seen, the configuration HRP/Au_{c5}/DAB_4-SHFc/AuNPs/GCE (DAB-SHFc biosensor) shows the best results, followed by DAB-SH biosensor. For this reason, from now on, we will only report the results of these biosensors.

Next, the kinetic and analytical characterization of the DAB-SHFc biosensor was studied by amperometry at applied potential − 0.3 V, selected as optimum to carry out the direct electrochemistry of HRP. Fig. S5 shows both the calibration plot and the corresponding double reciprocal Lineweaver–Burk plot, which allow us to know the analytical and kinetic parameters. In addition, the inset in Fig. S5a demonstrates that the amperometric response of the biosensor to hydrogen peroxide is

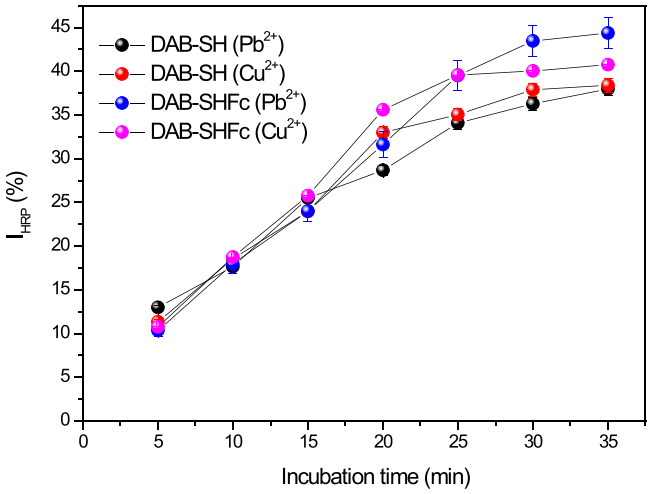

Fig. 8. Percent inhibition of DAB-SH and of DAB-SHFc biosensors exposed at 0.05 mM of Pb^{2+} or Cu^{2+} during several incubation times. All measured at − 0.3 V in PBS pH 7.0 with H_2O_2 0.1 mM. The error bars show the ± SD (n = 3).

very fast, reaching the stationary value in a period of 2–3 s. In the same way as the DAB-SH biosensors [32], the DAB-SHFc biosensor shows three linear ranges (at least until 5 mM) between 0 and 200 μM; 200 – 1000 μM and 1000 – 5000, with sensitivities of 675.0; 596.8 and 489.8 μA mM^{-1} cm^{-2}, respectively. The LOD, calculated as three times the standard deviation was 11 nM.

The Lineweaver–Burk plots allow us to obtain the apparent overall rate constant, k_{app}, and the apparent Michaelis constant, K'_M, whose values obtained for the DAB-SHFc biosensor were 0.050 A M^{-1} and 4.46 mM respectively. These values are higher than those obtained for the DAB-SH biosensor (0.047 A M^{-1} and 1.16 mM respectively), indicating that the presence of ferrocene in the dendrimer provides a faster overall reaction rate. The higher K'_M value could be related with a lower effective enzymatic catalysis, however, the little increase relative to the intrinsic value (3.70 mM) [56] indicates that the biosensor shows an effective enzyme catalysis and that their structure in relation to the DAB-SH biosensor is a little different. Note that K'_M is an apparent constant and their values can change with the structure of each biosensor, and so cannot be strictly compared. Savinell et al. [57] developed a Lineweaver-Burk-based model that allows identifying the rate-limiting step of the overall enzyme-catalysed reaction at the modified electrodes. The obtained double reciprocal plot is a straight line, in the same way as the DAB-SH biosensors. According to Savinell's model, in this case, the overall reaction rate is limited by a combination of the enzyme catalysis and the electron mediation steps. Consequently, the diffusion and electrolysis are fast enough, confirming that the applied potential of − 0.3 V is adequate.

All these results are certainly promising for the development of new biosensors based on the inhibition of the enzyme due to the presence of heavy metals.

3.3. HRP inhibition

The bioelectrocatalytic mechanism of immobilized HRP is usually expressed by the scheme [58,59]:

$$\text{HRP-Fe(III)} + H_2O_2 \rightarrow \text{Compound I (Fe(IV) = O)} + H_2O$$

$$\text{Compound I (Fe(IV) = O)} + 2e^- + 2\,H^+ \rightarrow \text{HRP[Fe(III)]} + H_2O$$

If an inhibitor is present in the medium, it can interact with the active

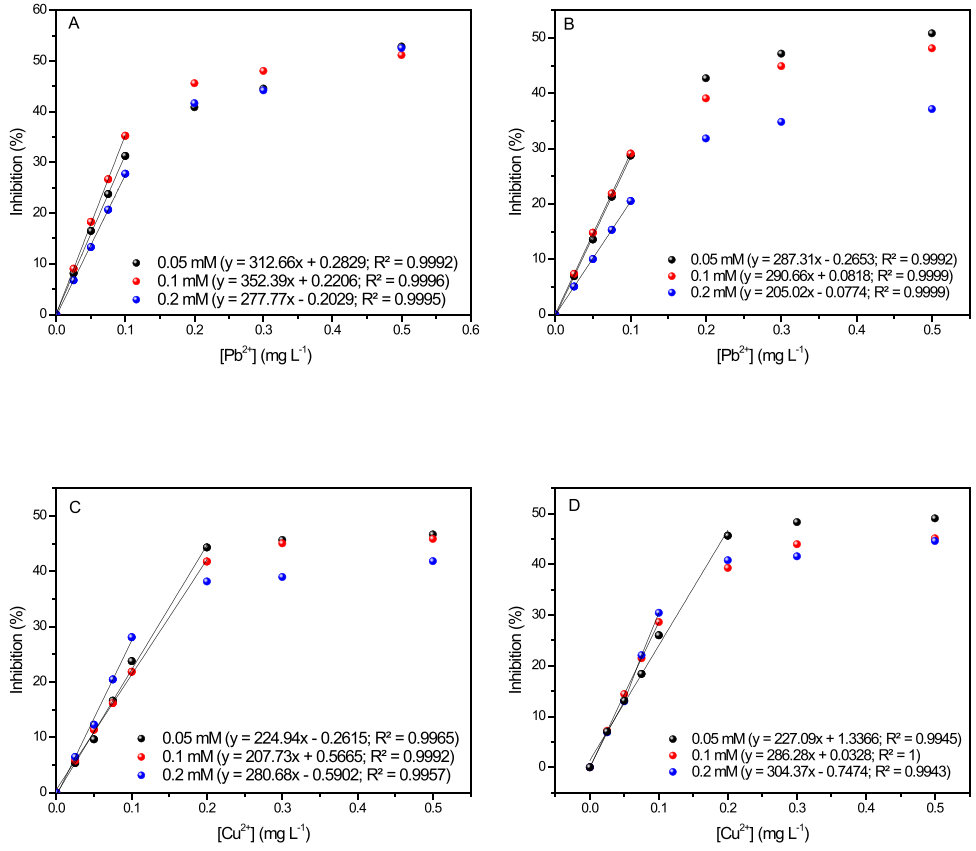

Fig. 9. Calibration curves for HRP inhibition by Pb^{2+} at DAB-SH (A) and DAB-SHFc (B), and Cu^{2+} at DAB-SH (C) and DAB-SHFc (D) biosensors. All measured at − 0.3 V in PBS pH 7.0, incubation time of 10 min at several H_2O_2 concentrations.

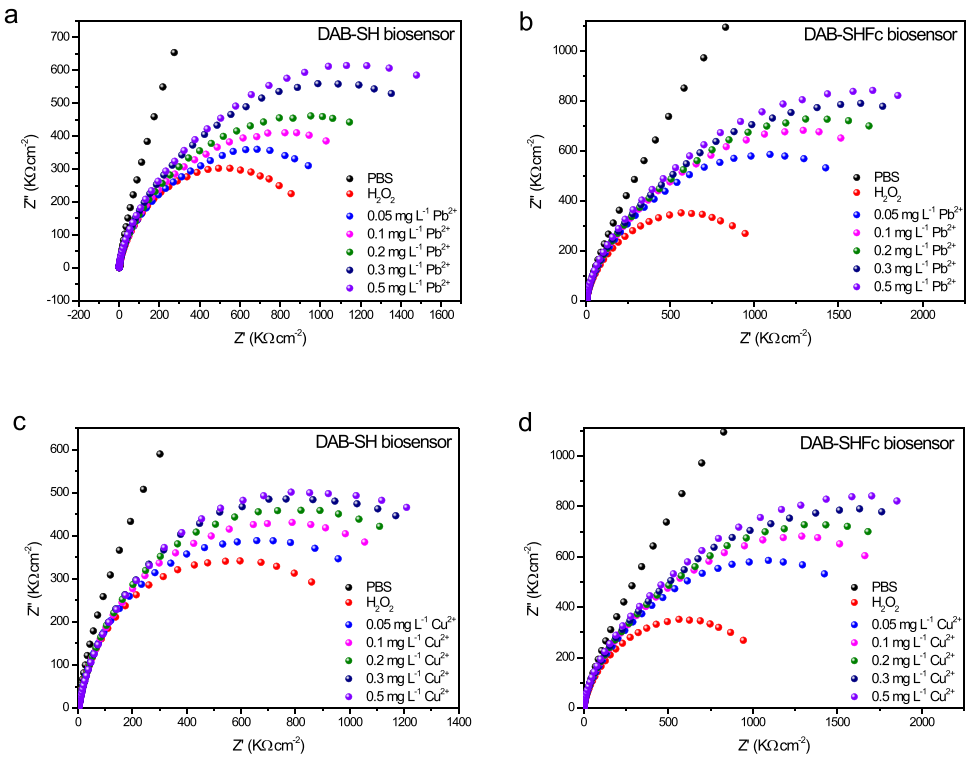

Fig. 10. Impedance spectra of DAB-SH and DAB-SHFc biosensors in PBS, and in presence of H_2O_2 1 mM without and with several quantities of Pb^{2+} (a and b) or Cu^{2+} (c and d), after 10 min of incubation time.

site or other of HRP, resulting in a loss of activity that causes the subsequent decrease in the electrochemical signal. This decrease is directly related with the inhibitor concentration and with the time of exposure to it, therefore, its measurement can be used as sensing tool.

3.3.1. *Effect of incubation time*

Usually, the interaction enzyme-inhibitor is slower than that enzyme-substrate, and so the study of the incubation time is essential to develop a new device based on inhibition. For this purpose, different essays were carried out by measuring the amperometric response after several incubation times in solutions containing 0.05 mg/L of Pb^{2+} or Cu^{2+} respectively. Usually, the concentration of metals in the incubation studies for sensing applications are in a 0.5 – 1 mg/L range [58,60]. We have selected a significantly lower concentration to prove that our biosensors allow us to detect earlier inhibitions than previous developments. The measurements were made in PBS 0.1 M pH 7 solution containing 0.1 mM of substrate H_2O_2. The HRP percentage of inhibitions (*% I_{HRP}*) were calculated by the equation [58]: *% $I_{HRP} = 100\ x\ (I_i - I_f)/I_i$*, being I_i the biosensor response obtained in absence of inhibitor and I_f the response obtained after each incubation period. Fig. 8 shows the results obtained with both biosensors in presence of Pb^{2+} or Cu^{2+} at incubation times between 0 and 35 min. As expected, the increase in the incubation time also increases the inhibition percentages and no significant differences were observed at both type of biosensors. The LOD decreases and the inhibition grade increases with the increasing incubation time [60] and so, an inhibition time that allows achieving a *% $I_{HRP} > 10\%$* is usually selected to obtain low LOD. In our case, *%$I_{HRP} > 10\%$* is reached in all the cases after an incubation time of 5 min (11.3% for Cu^{2+} and 13% for Pb^{2+} with the DAB-SH biosensor and 10.8% for Cu^{2+} and 10.3% for Pb^{2+} with the DAB-SHFc one). Consequently, we selected an incubation time of 10 min in order to obtain low LOD, higher *%I_{HRP}*, and short analysis time.

3.3.2. *Effect of H_2O_2 concentration*

The amount of substrate H_2O_2 can substantially influence percent inhibition. On the one hand, a high concentration of substrate can decrease the inhibition by displacement of the inhibitor that competes with it. On the other hand, if the substrate concentration is low, the response current decreasing could not be observed due to the substrate easy catalytic reduction. Fig. 9 shows the responses to several concentrations of Pb^{2+} and Cu^{2+} of the DAB-SH and DAB-SHFc biosensors with H_2O_2 substrate concentrations of 0.05, 0.1 and 0.2 mM. As it can be seen, the Pb^{2+} determination shows a linear relation to 0.1 mg/L with both biosensors and the best sensitivity is obtained in 0.1 mM of substrate. Nevertheless, the Cu^{2+} presents different linear ranges as a function of the peroxide concentration and the type of biosensor. The limits of detection (LOD), obtained with both types of biosensors in presence of peroxide 0.1 mM, were 1.9 μg/L and 0.8 μg/L for the determination of Pb^{2+} with DAB-SH and DAB-SHFc, respectively, and 8.2 μg/L and 0.3 μg/L for Cu^{2+} respectively. The presence of ferrocene in the biosensor does not seem significant or determinant for the inhibition of the enzyme, however, the Fc-biosensors showed noticeable decrease in the LOD.

3.3.3. *Study on the HRP inhibition type*

The mode of how the enzyme is inhibited depends on the inhibitor, and the inhibition could be competitive, non-competitive, uncompetitive, or mixed [58]. The study of the type of inhibition was carried out through amperometric measurements with both biosensors in the presence of 0.05, 0.1 and 0.2 mM of H_2O_2, with increasing concentrations of metal ions. The type of inhibition was characterized by using Dixon (current^{-1} vs. metal concentration) and the Cornish-Bowden ([H_2O_2]/current vs. metal concentration) plots [61,62] (Figs. S6 and S7) obtained with both biosensor types. In all the cases, the Dixon plots showed the intersection of the lines in a point included in the second quadrant, while the Cornish-Bowden plot showed three parallel lines, indicative of competitive inhibition. In these cases, the value of the apparent inhibition constant K_i can be calculated from the intercept of lines in the Dixon plot. The results were very similar in all the cases, obtaining K_i values of 0.21 and 0.22 mg/L for the inhibition by Pb^{2+} at

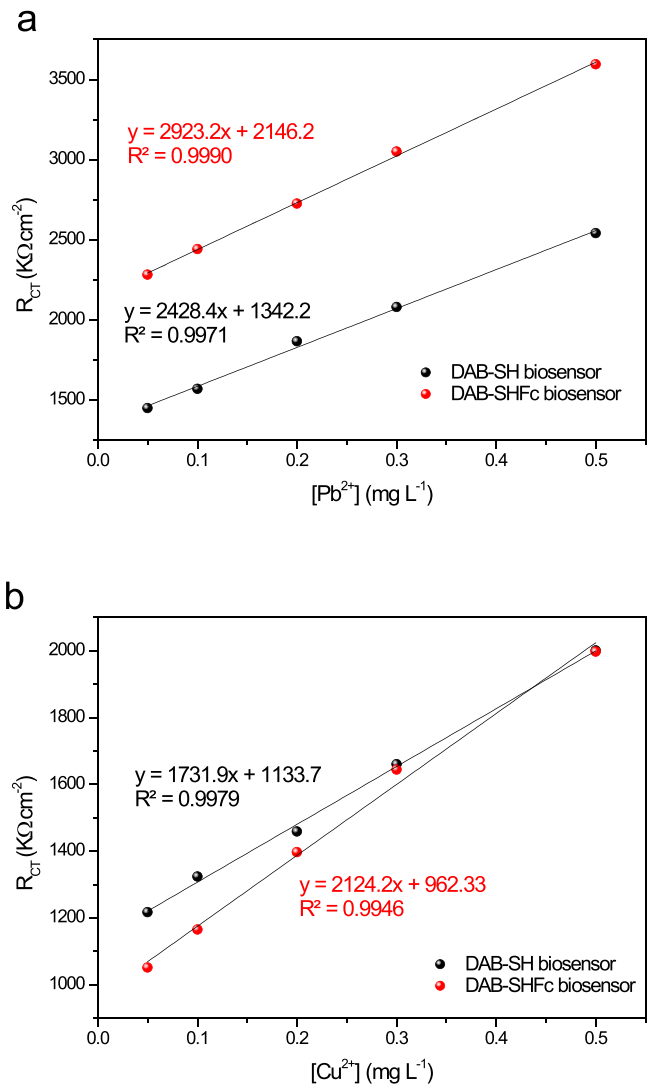

Fig. 11. Calibration EIS curves for HRP inhibition by (a) Pb^{2+} at DAB-SH and DAB-SHFc, and (b) Cu^{2+} at DAB-SH and DAB-SHFc biosensors. All measured at − 0.3 V in PBS pH 7.0, incubation time of 10 min with H_2O_2 1 mM. R_{CT} measured by the electrochemical circle fit (NOVA software) with a typical Randles equivalent circuit.

DAB-SH and DAB-SHFc biosensors respectively; and 0.21 and 0.20 for the inhibition by Cu^{2+} at the same biosensores, respectively.

3.3.4. *Impedimetric biosensor*

In recent years, EIS has demonstrated to be also useful to develop inhibition biosensors [60]. The incorporation of inhibitors to the enzyme structure causes changes in the charge transfer resistance, R_{CT}, which can be measured and related to the inhibitor concentration. Both selected biosensors have been studied in PBS at − 0.3 V vs SCE, with incubation time of 10 min and after addition of H_2O_2. Fig. 10 show the obtained spectra and Fig. 11 shows the linear dependence of R_{CT} with the metal ion concentration in the linear ranges.

Curiously, in this case, an increase in the sensitivity (slopes) of the biosensors that contain ferrocene is observed with respect to the DAB-SH one. In addition, the dependence of EIS measurements (R_{CT}) on the metal ion concentration showed wider linear intervals than the amperometric ones, and higher slopes, indicating a higher sensitivity. Consequently, the impedimetric biosensors were more useful than the classic amperometric devices at the same applied potential, and the DAB-SHFc dendrimer provides an interesting improvement compared to DAB-SH.

4. Conclusions

In this work, we have compared two ferrocenyl thiolated DAB dendrimers with their thiolated DAB homologues as bonding-layer between electrodeposited and colloidal gold nanoparticles. We have compared their electrocatalytic properties and carried out the complete electrochemical, kinetic and analytical characterization of modified electrodes to be used as biosensors for the determination of Pb^{2+} and Cu^{2+} based on their inhibitor effect of HRP. Both ions showed a competitive inhibition characterized by Dixon and Cornish-Bowden plots. The inhibition constants obtained from the Dixon plot were 0.21 mg/L and 0.22 mg/L for the Pb^{2+} inhibition with the DAB-SH and DAB-SHFc biosensors respectively; and 0.21 mg/L and 0.20 mg/L for the inhibition by Cu^{2+} respectively. The best results were obtained with the biosensors with configurations HRP/Au_{c5}/DAB_4-SHFc/AuNPs/GCE (DAB-SH biosensor) and HRP/Au_{c16}/DAB_{16}-SH/AuNPs/GCE (DAB-SHFc biosensor) and they were studied to develop both amperometric and impedimetric biosensors based on the inhibition of HRP. The best of the characterized biosensor was the impedimetric DAB-SHFc biosensor, that allows to determine Pb^{2+} and Cu^{2+} with low detection limits of 0.8 μg/L and 0.3 μg/L respectively in a wide linear range.

CRediT authorship contribution statement

Evelyn Ospina: Formal analysis. **Beatriz Alonso:** Methodology, Investigation, Supervision, Writing – review & editing. **Carmen M. Casado:** Methodology, Investigation, Supervision, Writing – review & editing. **M. Pilar García Armada:** Conceptualization, Data curation, Funding acquisition, Investigation, Methodology, Project administration, Supervision, Validation, Writing – original draft, Writing – review & editing.

Declaration of Competing Interest

The authors declare that they have no known competing financial interests or personal relationships that could have appeared to influence the work reported in this paper.

Data Availability

No data was used for the research described in the article.

Acknowledgements

The authors thank the ICTS Centro Nacional de Microscopia Electrónica de la Universidad Complutense de Madrid for assistance in the SEM studies. M. Pilar García Armada also thanks to the Madrid Government (Comunidad de Madrid, Spain) under the Multiannual Agreement with the Universidad Politécnica de Madrid in the Excellence Program for University Professors, in the context of V PRICIT (Regional Program of Research and Technological Innovation) by the financial support of this work.

This paper is dedicated to our appreciated colleague Professor David Tudela, on the occasion of his retirement.

Appendix A. Supporting information

Supplementary data associated with this article can be found in the online version at doi:10.1016/j.cattod.2023.114293.

References

[1] E. Kerek, M. Hassanin, E.J. Prenner, Inorganic mercury and cadmium induce reigidity in eukarytic lipid extracts while mercury also ruptures red blood cells, Biochim. Biophys. Acta Biomembr. 2018 (1860) 710–717, https://doi.org/10.1016/j.bbamem.2017.12.014.

[2] I.P.S. Fernando, K.K.A. Sanjeewa, S.Y. Kim, J.S. Lee, Y.J. Jeon, Reduction of heavy metal (Pb^{2+}) biosorption in zebrafish model using alginic acid purified from Ecklonia cava and two of its synthetic derivatives, Int. J. Biol. Macromol. 106 (2018) 330–337, https://doi.org/10.1016/j.ijbiomac.2017.08.027.

[3] M.B. Gumpu, S. Sethuraman, U.M. Krishnan, J. Rayappan, A review on detection of heavy metal ions in water - An electrochemical approach, Sens. Actuators B 213 (2015) 515–533, https://doi.org/10.1016/j.snb.2015.02.122.

[4] Z. Dahaghin, H.Z. Mousavi, S.M. Sajjadi, A novel magnetic ion imprinted polymer as a selective magnetic soils phase for separation of trace lead (II) ions from agricultural products, and optimization using a Box-Behnken design, Food Chem. 237 (2017) 275–281, https://doi.org/10.1016/j.foodchem.2017.05.118.

[5] H.A. Godwin, The biological chemistry of lead, Curr. Opin. Chem. Biol. 5 (2001) 223–227, https://doi.org/10.1016/S1367-5931(00)00194-0.

[6] R. Pratiwi, M.P. Nguyen, S. Ibrahim, N. Yoshika, C.S. Henry, D.H. Tjahjono, A selective distance-based paper analytical device for copper (II) determination using porphyrin derivative, Talanta 174 (2017) 493–499, https://doi.org/10.1016/j.talanta.2017.06.041.

[7] S. Abbasi, H. Khani, R. Tabaraki, Determination of ultra trace levels of copper in food samples by a highly sensitive adsorptive stripping voltammetric method, Food Chem. 123 (2010) 507–512, https://doi.org/10.1016/j.foodchem.2010.03.04.

[8] X. Niu, Y. Zhong, R. Chen, F. Wang, Y. Liu, D. Luo, A "turn-on" fluorescence sensor for Pb^{2+} detection based on grahene quantum dots and gold nanoparticles, Sens. Actuators B 255 (2018) 1577–1581, https://doi.org/10.1016/j.snb.2017.08.167.

[9] J.H. Kim, S.H. Han, B.H. Chung, Improving Pb^{2+} detection using DNAzyme-based fluorescence sensors by pairing fluorescence donors with gold nanoparticles, Biosens. Bioelectron. 26 (2011) 2125–2129, https://doi.org/10.1016/j.bios.2010.09.018.

[10] T. Priya, N. Dhanalakshmi, S. Thennarasu, N. Thinakaran, A nobel voltametric sensor for the simultaneous detection of Cd^{2+} and Pb^{2+} using graphene oxide/k-carrageena/L-cysteine nanocomposite, Carbohydr. Polym. 182 (2018) 199–206, https://doi.org/10.1016/j.carbpol.2017.11.017.

[11] M.A. Chamjangali, S. Boroumand, G. Bagherian, N. Goudarzi, Construction and characterization a non-amalgamation voltammetric flow sensor for online simultaneous determination of lead and cadmium ions, Sens. Actuators B 253 (2017) 124–136, https://doi.org/10.1016/j.snb.2017.06.098.

[12] B.C. Janegitz, L.H. Marcolino-Junior, S.P. Campana-Filho, R.C. Faria, O. Fatibello-Filho, Anodic stripping voltammetric determination of copper(II) using a functionalized carbon nanotubes paste electrode modified with crosslinked chitosan, Sens. Actuators B 142 (2009) 260–266, https://doi.org/10.1016/j.snb.2009.08.033.

[13] A.U. Rehman, M. Ikram, K. Kan, Y. Zhao, W.J. Zhang, J. Zhang, Y. Liu, Y. Wang, L. Dud, K. Shi, 3D Interlayer nanohybrids composed of reduced grapheneschemeoxide/SnO2/PPy grown from expanded graphite for the detection of ultra-trace Cd^{2+}, Cu^{2+}, Hg^{2+} and Pb^{2+} ions, Sens. Actuators B 274 (2018) 285–295, https://doi.org/10.1016/j.snb.2018.08.004.

[14] E.Y. Frag, M.E.B. Mohamed, E.M. Fahim, Application of carbon sensors for potentiometric determination of copper(II) in water and biological fluids of Wilson disease patients. Studying the surface reaction using SEM, EDX, IR and DFT, Biosen. Bioelectron. 118 (2018) 122–128, https://doi.org/10.1016/j.bios.2018.07.024.

[15] S. Li, F. Zhang, L. Chen, H. Zhang, H. Li, Nickel oxyhydroxide-functionalized n-silicon photoelectrode for the photocurrent determination of Hg(II) ions at zero working voltage, Sens. Actuators B 257 (2018) 9–15, https://doi.org/10.1016/j.snb.2017.10.125.

[16] Z. Li, J. Chen, M. Liu, Y. Yang, Supramolecular solvent-based micro extraction of copper and lead in water samples prior to reacting with synthesized Schiff base by flame atomic absorption spectrometry determination, Anal. Methods 6 (2014) 2294–2298, https://doi.org/10.1039/C3AY00065F.

[17] S. Su, B. Chen, M. He, B. Hu, Graphene oxide-silica composite coating hollow fiber solid phase microextraction online coupled with inductively coupled plasma mass spectrometry for the determination of trace heavy metals in environmental water samples, Talanta 123 (2014) 1–9, https://doi.org/10.1016/j.talanta.2014.01.061.

[18] M.E. Ghica, R.C. Carvalho, A. Amine, C.M.A. Brett, Glucose oxidase enzyme inhibition sensors for heavy metals at carbon film electrodes modified with cobalt or copper hexacyanoferrate, Sens. Actuator B: Chem. 178 (2013) 270–278, https://doi.org/10.1016/j.snb.2012.12.113.

[19] D. Bagal-Kestwal, M.S. Karve, B. Kakade, V.K. Pillai, Invertase inhibition based electrochemical sensor for thedetectionofheavymetalions inaqueous system: application of ultra-microelectrode to enhance sucrose biosensor's sensitivity, Biosens. Bioelectron. (2008) 657–664, https://doi.org/10.1016/j.bios.2008.06.027.

[20] P.N. Nomngongo, J.C. Ngila, V.O. Nyamori, E.A. Songa, E.I. Iwuoha, Determination of selected heavy metals using amperometric horseradish peroxidase (HRP) inhibition biosensor, Anal. Lett. 44 (2011) 2031–2046, https://doi.org/10.1080/00032719.2010.539738.

[21] C. Chen, X. Hong, T. Xu, A. Chen, L. Lu, Y. Gao, Hydrogen peroxide biosensor based on the immobilization of horseradish peroxidase onto a poly(aniline-co-N-methylthionine) film, Synth. Met. 212 (2016) 123–130, https://doi.org/10.1016/j.msec.2016.01.058.

[22] H. Hamidi, B. Haghighi, Fabrication of a sensitive amperometric sensor for NADH and H_2O_2 using palladium nanoparticles-multiwalled carbon nanotube nanohybrid, Mat. Sci. Eng. C 62 (2016) 423–428, https://doi.org/10.1016/j.msec.2016.01.058.

[23] M.P. Garcia Armada, J. Losada, I. Cuadrado, B. Alonso, B. Gonzalez, C.M. Casado, J. Zhang, Preparation of biosensors based in a siloxane homopolymer with interacting ferrocenes for the amperometric detection of peroxides, Sens. Actuators B 101 (2004) 143, https://doi.org/10.1016/j.snb.2004.02.043.

[24] J. Losada, M. Zamora, M.P. Garcia Armada, I. Cuadrado, B. Alonso, C.M. Casado, Bienzyme sensors based on novel polymethylferrocenyl dendrimers, Anal. Bioanal. Chem. 385 (2006) 1209, https://doi.org/10.1007/s00216-006-0330-8.

[25] M. Li, S. Xu, M. Tang, L. Liu, F. Gao, Y. Wang, Direct electrochemistry of horseradish peroxidase on graphene-modified electrode for electrocatalytic reduction towards H_2O_2, Electrochem. Acta 56 (2011) 1144–1149, https://doi.org/10.1016/j.electacta.2010.10.034.

[26] Y. Wang, Z. Wang, Y. Rui, M. Li, Horseradish peroxidase immobilization on carbon nanodots/CoFe layers double hydroxides: Direct electrochemistry and hydrogen peroxide sensing, Biosens. Bioelectron. 64 (2015) 57–62, https://doi.org/10.1016/j.bios.2014.08.054.

[27] E. Ospina, M.P. Garcia Armada, J. Losada, B. Alonso, C.M. Casado, Polyferrocenyl polycyclosiloxane/gold nanoparticles: an efficient electrocatalytic platform for immobilization and direct electrochemistry of HRP, J. Electrochem. Soc. 163 (2016) H826–H833, https://doi.org/10.1149/2.1141609jes.

[28] M. Moyo, J.O. Okonkwo, Horseradish peroxidase biosensor based on maize tassel–MWCNTs composite for cadmium detection, Sens. Actuators B 193 (2014) 515–521, https://doi.org/10.1016/j.snb.2013.11.086.

[29] P.N. Nomngongo, J.C. Ngila, V.O. Nyamori, E.A. Songa, E.I. Iwuoha, Determination of selected heavy metals using amperometric horseradish peroxidase (HRP) inhibition biosensor, Anal. Lett. 44 (2011) 2031–2046, https://doi.org/10.1080/00032719.2010.539738.

[30] P.N. Nomngongo, J.C. Ngila, T.A.M. Msagati, Indirect amperometric determination of selected heavy metals based on horseradish peroxidase modified electrodes, ISBN: 978-953-307-328-6, in: P.A. Serra (Ed.), Biosensors - Emerging Materials and Applications, InTech, 2011.

[31] A. Attara, M.E. Ghicaa, A. Amine, C.M.A. Brett, Poly(neutral red) based hydrogen peroxide biosensor for chromiumdetermination by inhibition measurements, J. Hazard. Mater. 279 (2014) 348–355, https://doi.org/10.1016/j.jhazmat.2014.07.019.

[32] E. Ospina, C.M. Casado, B. Alonso, M.P. García Armada, Thiolated DAB dendrimers-gold nanoparticles as self-assembled layers for the direct electrochemistry of HRP, J. Electrochem. Soc. 166 (15) (2019) B1434–B1440, https://doi.org/10.1149/2.0411915jes.

[33] T. Tatsuma, Y. Okawa, T. Watanabe, Enzyme monolayer- and bilayer-modified tin oxide electrodes for the determination of hydrogen peroxide and glucose, Anal. Chem. 61 (1989) 2352, https://doi.org/10.1021/ac00196a007.

[34] A. Mulchandani, W. Chia-Ling, Bienzyme sensors based on poly (anilinomethylferrocene)-modified electrodes, Electroanalysis 8 (1996) 414, https://doi.org/10.1002/elan.1140080503.

[35] J. Losada, M. Zamora, M.P. García Armada, I. Cuadrado, B. Alonso, C.M. Casado, Bienzyme sensors based on novel polymethylferrocenyl dendrimers, Anal. Bioanal. Chem. 385 (2006) 1209–1217. Doi.org/10.1007/s00216-006-0330-8.

[36] B. Alonso, C.M. Casado, I. Cuadrado, M. Morán, A.E. Kaifer, Effective recognition of $H_2PO_4^-$ by a new series of dendrimers functionalised with ferrocenyl-urea termini, Chem. Commun. (2002) 1178–1779, https://doi.org/10.1039/b205619d.

[37] M. Algarra, B. Campos, B. Alonso, M.S. Miranda, A.M. Martínez, C.M. Casado, J.C.G. Esteves da Silva, Thiolated DAB dendrimers and CdSe quantum dots nanocomposites for Cd(II) or Pb(II) sensing, Talanta 88 (2012) 403–407, https://doi.org/10.1016/j.talanta.2011.11.007.

[38] H. Yin, S. Ai, W. Shi, L. Zhu, A novel hydrogen peroxide biosensor based on horseradish peroxidase immobilized on gold nanoparticles-silk fibroin modified glasy carbon electrode and direct electrochemistry of horseradish peroxidase, Sens. Actuators B 137 (2009) 747–753, https://doi.org/10.1016/j.snb.2008.12.046.

[39] K. Schlögl, H. Seiler, Ferrocenyl-isocyanat, Naturwissenschaften 45 (1958) 337, https://doi.org/10.1007/BF00640223.

[40] S. Connolly, S.N. Rao, D. Fitzmaurice, Characterization of protein aggregated gold nanoparticles, J. Phys. Chem. B 104 (2000) 4765–4776, https://doi.org/10.1021/jp992842u.

[41] F.S. Arimoto, A.C. Haven, Derivates of dicyclopentadienyliron, J. Am. Chem. Soc. 77 (1955) 6295–6297, https://doi.org/10.1021/ja01628a068.

[42] X. Kang, J. Wang, Z. Tang, H. Wu, Y. Lin, Direct electrochemistry and electrocatalysis of horseradish peroxidase immobilized in hybrid organic-inorganic film of chitosan/sol-gel/carbon nanotubes, Talanta 78 (2009) 120–125, https://doi.org/10.1016/j.talanta.2008.10.063.

[43] J. Wang, L. Wang, J. Di, Y. Tu, Electrodeposition of gold nanoparticles on indium/tin oxide electrode for fabrication of a disposable hydrogen peroxide biosensor, Talanta 77 (2009) 1454–1459, https://doi.org/10.1016/j.talanta.2008.09.034.

[44] Q. Wan, H. Song, H. Shu, Z. Wang, J. Zou, N. Yang, In situ synthesized gold nanoparticles for direct electrochemistry of horseradish peroxidase, Colloids Surf. B Biointerfaces 104 (2013) 181–185, https://doi.org/10.1016/j.colsurfb.2012.12.009.C.

[45] H. Cai, C. Xu, P. He, Y. Fang, Colloid Au-enhanced DNA immobilization for the electrochemical detection of sequence-specific DNA, J. Electroanal. Chem. 510 (2001) 78–85, https://doi.org/10.1016/S0022-0728(01)00548-4.

[46] O.S. Ivanova, F.P. Zamborini, Electrochemical size discrimination of gold nanoparticles attached to glass/indium-tin-oxide electrodes by oxidation in bromide-containing electrolyte, Anal. Chem. 82 (2010) 5844–5850, https://doi.org/10.1021/ac101021q.

[47] P.R. Chandran, M. Naseer, N. Udupa, N. Sandhyarani, Size controlled synthesis of biocompatible gold nanoparticles and their activity in the oxidation of NADH, Nanotechnology 23 (2012), 015602, https://doi.org/10.1088/0957-4484/23/1/015602.

[48] R. Segura, J. Pizarro, K. Díaz, A. Placencio, F. Godoy, E. Pino, F. Recio, Development of electrochemical sensors for the determination of selenium using gold nanoparticles modified electrodes, Sens. Actuators B 220 (2015) 263–269, https://doi.org/10.1016/j.snb.2015.05.016.
[49] S. Trasatti, O.A. Petrii, Real surface area measurements in electrochemistry, Pure Appl. Chem. 63 (1991) 711–734, https://doi.org/10.1351/pac199163050711.
[50] D.F. Yancey, L. Zhang, R.M. Crooks, G. Henkelman, Au@Pt dendrimer encapsulated nanoparticles as model electrocatalysts for comparison of experiment and theory, Chem. Sci. 3 (2012) 1033–1040, https://doi.org/10.1039/C2SC00971D.
[51] E. Laviron, General expression of the linear potential sweep voltammogram in the case of diffusionless electrochemical systems, J. Electroanal. Chem. 19 (1979), https://doi.org/10.1016/S0022-0728(79)80075-3.
[52] E. Katz, I. Willner, Probing biomolecular interactions at conductive and semiconductive surfaces by impedance spectroscopy: routes to impedimetric immunosensors, dna-sensors, and enzyme biosensors, Electroanalysis 15 (2003) 913–947, https://doi.org/10.1002/elan.200390114.
[53] K. Thenmozhi, S.S. Narayanan, Horseradish peroxidase and toluidine blue covalently immobilized leak-free sol-gel composite biosensor for hydrogen peroxide, Mater. Sci. Eng. C 70 (2017) 223–230, https://doi.org/10.1016/j.msec.2016.08.075.
[54] Y. Xin, X. Fu-bing, L. Hong-wei, W. Feng, C. Di-zhao, W. Zhao-yang, A novel H_2O_2 biosensor based on Fe_3O_4-Au magnetic nanoparticles coated horseradish peroxidase and graphene sheets-Nafion film modified screen-printed carbon electrode, Electrochim. Acta 109 (2013) 750–755, https://doi.org/10.1016/j.electacta.2013.08.011.
[55] A.J. Bard, L.R. Faulkner, Electrochemical methods. Fundamentals and Applications, second ed., John Wiley & Sons, Inc, New York, 2001, p. 381. ISBN 0-471-04372-9.
[56] L. Gao, J. Zhung, L. Nie, J. Zhang, N. Gu, T. Wang, J. Feng, D. Yang, S. Perrett, X. Yan, Intrinsic peroxidase-like activity of ferromagnetic nano particles, Nat. Nanotechnol. 2 (2007) 577–583, https://doi.org/10.1038/nnano.2007.260.
[57] J. Ch, Ch Chen, C. Liu, R.F. Savinell, Polymeric redox mediator enzyme electrodes for anaerobic glucose monitoring, J. Electroanal. Chem. 348 (1993) 317–338, https://doi.org/10.1016/0022-0728(93)80140-D.
[58] M. Moyo, J.O. Okonkwo, N.M. Agyei, An amperometric biosensor based on horseradish peroxidase immobilized onto maize tassel-multi-walled carbon nanotubes modified glassy carbon electrode for determination of heavy metal ions in aqueous solution, Enzym. Microb. Tecnol. 56 (2014) 28–34, https://doi.org/10.1016/j.enzmictec.2013.12.014.
[59] F.W. Krainer, A. Glieder, An updated view on horseradish peroxidases: recombinant production and biotechnological applications, Appl. Microbiol Biotechnol. 99 (2015) 1611–1625, https://doi.org/10.1007/s00253-014-6346-7.
[60] B. Elsebai, M.E. Ghica, M.N. Abbas, C.M. A.Brett, Catalase based hydrogen peroxide biosensor for mercury determination by inhibition measurements, J. Hazard. Mater. 340 (2017) 344–350, https://doi.org/10.1016/j.jhazmat.2017.07.021.
[61] M. Dixon, The determination of enzyme inhibitor constants, Biochem. J. 55 (1953) 170–171, https://doi.org/10.1042/bj0550170.
[62] A. Cornish-Bowden, A simple graphical method for determining the inhibition constants of mixed, uncompetitive and non-competitive inhibitors, Biochem. J. 137 (1974) 143–144, https://doi.org/10.1042/bj1370143.